# Effect of viscous dissipation on the generation of shear flow at a plasma edge in the finite gyro-radius guiding center approximation

Physica Scripta. Vol. 55, 617–627, 1997

# Effect of Viscous Dissipation on the Generation of Shear Flow at a Plasma Edge in the Finite Gyro-Radius Guiding Center Approximation

M. Shoucri, J. Lebas, G. Knorr[2], P. Bertrand[1], A. Ghizzo[1], G. Manfredi, and I. Christopher[2]

Centre Canadien de Fusion Magnétique, Varennes, Québec, J3X 1S1, Canada

*Received May 5, 1996; revised version received August 19, 1996; accepted September 26, 1996*

**Abstract**

A numerical simulation is performed to study the effect of a viscous dissipation term on the generation of shear flow at a plasma edge in the guiding center approximation. The guiding center model includes the effects of finite Larmor radius corrections and polarization drift. The numerical code applies the method of fractional steps to the fluid guiding center equations. We attempt to discriminate between the smoothing of the microstructure by a small viscous dissipation term to control numerical instabilities, and the modification of the macroscopic physical results introduced by this small viscous dissipation term. The finite Larmor radius effect allows for a charge separation to exist, which can be further accentuated by the polarization drift. A difference in the viscous term between electrons and ions can add to the charge separation effect at the plasma edge, which can modify the physical results. The numerical calculation is effected using a slab model, periodic in one direction and finite in the other direction, with an inhomogeneous density of guiding centers to simulate a plasma edge. The evolution of the system shows the potential evolving to a shape characterized by the longest wavelength associated with the transverse dimension of the system, an evolution characteristic of an inverse cascade. We present an analysis of the effect of different values of the viscous term on the time evolution of this guiding center system, and on the formation and existence of a charge separation and an electric field at the edge of a plasma and the associated shear in the $\boldsymbol{E} \times \boldsymbol{B}$ flow.

## 1. Introduction

An important set of equations relevant to the plasma edge physics in a tokamak are the two-dimensional finite Larmor radius guiding center equations [1]. The effect of the finite Larmor radius is to allow for a charge separation between electrons and ions to exist in the $\boldsymbol{E} \times \boldsymbol{B}$ flow. A theoretical study of the asymptotic state of the finite Larmor radius system of guiding-center equations has been presented in Ref. [1]. It has three "rugged" invariants and it was shown that the canonical ensemble probability distribution for this system can have negative temperature states, characterized by an inverse energy cascade with energy accumulating in the low $k$ modes (the longest structures allowed consistent with the boundary conditions) in the asymptotic equilibrium. Once this stage has been reached, the energy remains in the lowest $k$ modes, and high $k$ modes fluctuations are negligible.

The two-dimensional finite Larmor radius guiding center model was extended in Ref. [2] by including the polarization drift, and a numerical code was developed to study the pertinent equations for the case of a plasma slab with an inhomogeneous density of guiding centers, to simulate a plasma edge. The polarization drift has a different sign for ions and electrons (but is smaller for electrons), and thus has a tendency to produce and accentuate a charge separation in a time varying electric field. The remarkable result of Ref. [2] was that the inverse cascade still exists in this model, with energy evolving to large structures which scale with the size of the system, while the system is evolving from an initial unstable flow with shear to a final more stable shear dominated flow. These longest wavelength transition results were studied in the presence of a self-consistent electric field and charge separation for a plasma edge. It was shown in Ref. [2] that during this evolution, fine structures develop in the density which causes the simulation to be unstable when these structures become of the order of the grid size. This problem was controlled by adding a viscosity term $\nu_{i,e}\nabla^2 n_{i,e}$ to the ions and electrons density equations, with $\nu_{i,e}$ small enough to provide the necessary dissipation for the short wavelengths developing in the system, without affecting the long wavelength modes of the large scales responsible for the macroscopic behavior of the system. The exact form of the dissipation may be unimportant, provided it prevents the unnatural reflection of fluctuations from the cutoff wavenumber, when the fluctuation wavelength becomes of the order of the grid size. This problem was discussed in Ref. [3] in connection with the solution of the 2-D guiding center equations, and in Refs. [4, 5] in connection with the problem of 2-D drift wave turbulence. More recently, results where presented in Ref. [6] with a hyper-viscosity term used in the simulation. However, the question arises whether in some cases the dissipation term can have some effect on the solution, or can significantly affect the solution. Some recent results presented in Ref. [7] show that even though the effect of a small viscous term have little effect on the asymptotic level of the dominant Fourier mode in the periodic direction, it does affect the transverse profile of the charge separation and associated potential at the plasma edge. Such effects have also been studied in 2-D resistive magnetohydrodynamic instabilities (see, for instance, Refs. [8, 9, 10]). It was stressed in Refs. [9 and 10] that any kind of smoothing may affect the resistive instabilities, and in Refs. [8 and 9] results for the evolution of the stream function were shown where the dynamics were described as an impulsive bursty reconnection. We note also the recent works in Ref. [11], where attention was focused on the role of viscosity in determining the existence and nonlinear evolution of instabilities.

We study in this work the effect of a viscosity term of the form $\nu_{i,e}\nabla^2 n_{i,e}$ added to the guiding center equations of the

[1] LPMI-URA 835 CNRS, Université Henri Poincaré, Nancy, France.
[2] Department of Physics and Astronomy, Univ. of Iowa, Iowa City, Iowa, U.S.A.

electrons and the ions respectively, as reported in Ref. [2]. In section 2, we present these equations. In section 3, we present the numerical code which consists in applying a method of fractional steps to the fluid guiding center equations. We run the code for sufficiently long time and study the effect of the viscous coefficient $\nu_{e,i}$ on the solution. These results are presented in section 4. Finally section 5 presents our conclusions.

## 2. The pertinent equations

The guiding center model with zero Larmor radius is given by [3, 12]:

$$\frac{\partial \rho}{\partial t} + \nabla \cdot (V_D \rho) = 0, \quad V_D = -\nabla\phi \times e_z/B, \quad \Delta\phi = -\rho/\varepsilon_0. \tag{1}$$

Here $\rho$ is the charge density, $V_D$ is the drift velocity and $\phi$ the electrostatic potential.

If we enforce periodic boundaries or enclose the plasma with metal walls of infinite conductivity, the energy theorem may be written as

$$W = \tfrac{1}{2}B^2\varepsilon_0 \int V_D^2 \, d\tau = \tfrac{1}{2}\varepsilon_0 \int E^2 \, d\tau. \tag{2}$$

The integral is the energy in the electrostatic field and the particle motion itself does not contribute to the energy. This is borne out by the fact that $W$ in eq. (2) is not proportional to the particle mass.

The finite Larmor radius model has been investigated in Ref. [1] and is given by

$$\frac{\partial n_e}{\partial t} + \nabla \cdot (\bar{V}_D n_e) = 0, \quad \frac{\partial n_i}{\partial t} + \nabla \cdot (\bar{V}_D n_i) = 0,$$

$$\Delta\phi = -q(\bar{n}_i - \bar{n}_e)/\varepsilon_0; \tag{3}$$

where $V_D = -\nabla\phi \times e_z/B$.

The bar over $V_D$ and $n_{i,e}$ is an abbreviation for an integral operation defined by

$$\bar{a}(r) = g \otimes a(r) = \int G(r - r')a(r') \, dr', \tag{4}$$

which takes into account that the guiding centers and particle locations are not the same. $G(r)$ is a symmetric kernel and $a(r)$ is an arbitrary function of $r$. The operator $g\otimes$ commutes with differential operators. In Fourier space the integral operator $g\otimes$ becomes a filtering operation, which is numerically easy to perform on the different Fourier modes [1, 13, 14]. Each coefficient $a_k$ of the mode $e^{ik\cdot r}$ is multiplied by a factor $g_k = \exp(-\frac{1}{2}k^2 r_{i,e}^2)$, where $k$ is the total wave vector and $r_{i,e}$ the Larmor radius (for ions or electrons respectively). This model can now represent guiding center density gradients, which was not possible in the zero Larmor radius model. The energy conservation becomes

$$W = \tfrac{1}{2}B^2\varepsilon_0 \int V_D^2 \, d\tau, \tag{5}$$

which is identical to the zero Larmor radius model. Again the motion of the particles does not contribute to the energy. It is therefore not surprising that the finite Larmor radius and the zero Larmor radius models are quite similar to each other. In particular, both have the possibility that, given certain initial conditions, energy can cascade to lower wave numbers, where it manifests itself macroscopically by the appearance of large scale structures. This effect is known as an inverse cascade.

The guiding center models with zero and finite Larmor radius possess two or more quadratic invariants which remain conserved if the system is truncated in Fourier space. In addition to energy, it is easy to show that the enstrophy $E$,

$$E = \int (\nabla \times V)^2 \, d\tau \tag{6}$$

is an invariant for the zero Larmor radius model. For the finite Larmor radius case, we have the invariants:

$$N_i = \int n_i^2 \, d\tau \quad \text{and} \quad N_e = \int n_e^2 \, d\tau. \tag{7}$$

A study of the asymptotic states of the finite Larmor radius system of equations has been presented in Ref. [1]. A canonical ensemble probability distribution characterized by the three invariants was derived, and it was shown that this system can have possible negative temperature states leading the energy to condense in the low $k$ modes.

Adding, as a final step, the polarization drift, we arrive at the model.

$$\frac{\partial n_e}{\partial t} + \nabla \cdot [(\bar{V}_D + \bar{V}_{pe})n_e] = 0,$$

$$\frac{\partial n_i}{\partial t} + \nabla \cdot [(\bar{V}_D + \bar{V}_{pi})n_i] = 0; \tag{8}$$

$$\Delta\phi = -\frac{q}{\varepsilon_0}(\bar{n}_i - \bar{n}_e).$$

with $\bar{a}(r) = g \otimes a(r)$, as defined in eq. (4) and

$$V_D = -\nabla\phi \times e_z/B, \tag{9}$$

$$V_{pv} = \frac{1}{\Omega_v^2}\frac{q_v}{m_v}\frac{d}{dt}E = \alpha_v\{\partial_t E + (V_{Dv} + V_{pv}) \cdot \nabla E\}. \tag{10}$$

where $v = i, e$ and $\alpha_v = \dfrac{1}{\Omega_v^2}\dfrac{q_v}{m_v}$, $q_i = q$ and $q_e = -q$.

Usually the polarization drift of the electrons is negligible because it is smaller by a factor of $(m_e/m_i)$ than the polarization drift of the ions. Note that the polarization drift in Eq. (10) is implicitly defined. We will discuss this point later.

The derivation of the energy theorem for this set of equations is found in Appendix I. The result is

$$W = \frac{1}{2}\int \left\{ \varepsilon_0 E^2 + \left(\frac{\omega_{pi}^2}{\Omega_i^2}\right)\frac{n_i}{n_0}(\bar{E}^i)^2 + \left(\frac{\omega_{pe}^2}{\Omega_e^2}\right)\frac{n_e}{n_0}(\bar{E}^e)^2 \right\} d\tau = \text{const.} \tag{11}$$

which can be written as

$$W = \frac{1}{2}\int \{\varepsilon_0 E^2 + m_i n_i (\bar{V}_{Di}^i)^2 + m_e n_e (\bar{V}_{De}^e)^2\} \, d\tau = \text{const.} \tag{12}$$

The first term is again the electrostatic field energy and the second and third terms are the particle energies of the ions and electrons, drifting with their respective drift velocities. The upper index indicates whether the averaging takes place

over an ion (i) or an electron (e) gyro-radius. Remarkably, the polarization drift does not appear in the energy theorem. All three models share the feature that the dipole moments formed by the rotating particles remain constant and therefore do not enter the energy equation.

It has been mentioned that eq. (10) defines $V_{pv}$ implicitly. The question arises whether this definition always has a unique solution for $V_{pv}$.

We rewrite eq. (10) for the ions as

$$V_p \cdot (I - \alpha_i \nabla E) = \alpha_i \left( \frac{\partial E}{\partial t} + V_D \cdot \nabla E \right).$$

Due to the electrostatic nature of $E$ the tensor $\nabla E$ is symmetric and can be transformed to principal axes, in which system the equation can immediatly be solved for $V_p$. We realize that our approximation is only meaningful if:

$$|\alpha \nabla E|_{max} < 1. \tag{13}$$

Only if the polarization drift is implicitly defined as in eq. (10) we get exact energy conservation. But then eq. (13) follows as a restriction of the model. In the present numerical simulations, the $V_{pv} \cdot \nabla E$ implicit term in eq. (10) has been omitted all together so that the question of a unique polarization drift and the validity of the model never arises. The energy conservation is then no longer an exact invariant of the system.

No additional quadratic invariants except the energy have been found for the model with polarization drift. However, it is perhaps the most significant result of the present work that, nevertheless, the numerical simulation shows the presence of an inverse cascade. It is to be noted that the polarization drift is generally small, and that the variation of the quantities in eq. (7) was slow during the simulation, and especially towards the end of the simulation. (Note that in the absence of polarization drift, the quantities in eq. (7) are exact invariants which are exactly conserved by the numerical code). The numerical results are discussed in details in the following section.

The model we study numerically in the present work is the same as the one presented in eqs. (8–10), with the addition of a viscosity term $\nu_{e,i} \nabla^2 n_{e,i}$ to the electrons and ions density equation respectively. Results presenting the effect of $\nu_{e,i}$ on the asymptotic solution are presented in Section 4. With $\nu_e = \nu_i = 7 \times 10^{-5}$, an initially neutral equilibrium is conserved, $V_{pv} = 0$ and the invariants in eq. (7) are exactly converved. The system remains in equilibrium. A small variation of $\nu_e$ with respect to $\nu_i$ can have important effects on charge neutrality at the edge and on the asymptotic electric field and asymptotic shear associated with the system. A small variation between $\nu_e$ and $\nu_i$ does more than simply smoothing the fine structure which develops during the time evolution of the system: it creates a charge separation at the plasma edge.

## 3. The Numerical Code

In the set of eqs (6)–(8), we use the following normalization:

- velocities are normalized to the ion thermal velocity $v_{thi}$,
- space is normalized to the ions gyro-radius $r_i = \frac{v_{thi}}{\Omega_i}$,
- time is normalized to $\Omega_i^{-1}$,
- potential is normalized to $T/e$, where $T$ is the temperature (we assume electrons and ions have the same temperature).

With this normalization, and with

$$E = -\nabla \phi \tag{14}$$

we have the following set of equations for the electrons (electrons gyro-radius correction is neglected):

$$\begin{aligned} &\frac{\partial n_e}{\partial t} + \left( E_y - \beta_e \frac{\partial E_x}{\partial t} - \beta_e E_y \frac{\partial E_x}{\partial x} + \beta_e E_x \frac{\partial E_x}{\partial y} \right) \frac{\partial n_e}{\partial x} \\ &\quad + \left( -E_x - \beta_e \frac{\partial E_y}{\partial t} - \beta_e E_y \frac{\partial E_y}{\partial x} + \beta_e E_x \frac{\partial E_y}{\partial y} \right) \frac{\partial n_e}{\partial y} \\ &\quad = + n_e \beta_e \frac{\partial}{\partial t} \left( \frac{\partial E_x}{\partial x} + \frac{\partial E_y}{\partial y} \right) + \nu_e \nabla^2 n_e \\ &\quad + n_e \beta_e \left( E_y \frac{\partial^2 E_x}{\partial x^2} - E_x \frac{\partial^2 E_y}{\partial y^2} + E_y \frac{\partial^2 E_x}{\partial y^2} - E_x \frac{\partial^2 E_y}{\partial x^2} \right) \end{aligned} \tag{15}$$

with

$$\beta_e = \frac{m_e}{m_i}. \tag{16}$$

The ion equation is similar, and is derived from eq. (15) by substituting $\beta_e$ by $(-1)$ and all the $E$ field components by the corresponding filtered values $\bar{E} \cdot \nu_e$ is substituted by $\nu_i$.

The numerical scheme uses a method of fractional steps and advances the equation as follows:

(1) Solve for $\Delta t/2$:

$$\frac{\partial n_e}{\partial t} + \left( E_y - \beta_e \frac{\partial E_x}{\partial t} - \beta_e E_y \frac{\partial E_x}{\partial x} + \beta_e E_x \frac{\partial E_x}{\partial y} \right) \frac{\partial n_e}{\partial x} = 0 \tag{17}$$

(with a similar equation for the ions).

The solution of eq. (17) is calculated by the shift

$$n_e^{*n+(1/2)} = n_e^n \left( y, x - \left( E_y^n - \beta_e \frac{\partial E_x^n}{\partial t} - \beta_e E_y^n \frac{\partial E_x^n}{\partial x} + \beta_e E_x^n \frac{\partial E_x^n}{\partial y} \right) \frac{\Delta t}{2} \right). \tag{18}$$

(The shift in eq. (18) is effected using a cubinc spline interpolatin [15]).

Then solve for $\Delta t/2$

$$\frac{\partial n_e^*}{\partial t} + \left( -E_x - \beta_e \frac{\partial E_y}{\partial t} - \beta_e E_y \frac{\partial E_y}{\partial x} + \beta_e E_x \frac{\partial E_y}{\partial y} \right) \frac{\partial n_e^*}{\partial y} = 0 \tag{19}$$

(with a similar equation for the ions).

The solution of eq. (19) is calculated by the shift

$$n_e^{n+(1/2)} = n_e^{*n+(1/2)} \times \left( x, y + \left( E_x^n + \beta_e \frac{\partial E_y^n}{\partial t} + \beta_e E_y^n \frac{\partial E_y^n}{\partial x} - \beta_e E_x^n \frac{\partial E_y^n}{\partial y} \right) \frac{\Delta t}{2} \right). \tag{20}$$

(2) Solve Poisson equation to update the electric field. (This equation is solved using the method presented in Ref.

[16] with zero boundary conditions for $\phi$). In our dimensionless units, this equation is written:

$$\Delta\phi = -\omega_{pi}^2(\bar{n}_i - n_e) \tag{21}$$

where $\omega_{pi}$ is normalized to $\Omega_i$. Note how sensitive is the charge in eq. (21) to the parameter $\omega_{pi}^2$.

Solve for $\Delta t$ the equation:

$$\frac{1}{n_e}\frac{\partial n_e}{\partial t} = \beta_e \frac{\partial}{\partial t}\left(\frac{\partial E_x}{\partial x} + \frac{\partial E_y}{\partial y}\right) + \beta_e\left(E_y \frac{\partial^2 E_x}{\partial x^2} - E_x \frac{\partial^2 E_y}{\partial y^2} + E_y \frac{\partial^2 E_x}{\partial y^2} - E_x \frac{\partial^2 E_y}{\partial x^2}\right) + \nu_e \nabla^2 n_e/n_e \tag{22}$$

(with a similar equation for the ions).

The solution of eq. (22) is given by:

$$n_e^+ = n_e^- \exp\left\{+\beta_e\left[\frac{\partial E_x^+}{\partial x} - \frac{\partial E_x^-}{\partial x} + \frac{\partial E_y^+}{\partial y} - \frac{\partial E_y^-}{\partial y}\right] + \nu_e \Delta t \nabla^2 n_e^-/n_e^- + \beta_e \Delta t \times \left(E_y \frac{\partial^2 E_x}{\partial x^2} - E_x \frac{\partial^2 E_y}{\partial y^2} + E_y \frac{\partial^2 E_x}{\partial y^2} - E_x \frac{\partial^2 E_y}{\partial x^2}\right)\right\}. \tag{23}$$

The subscripts + and − denote the values at the present and previous time steps respectively.

(3) Repeat Step 1.

The calculation of the spatial derivatives of the electric field is effected using cubic spline relations for the derivatives as explained in Ref. [17].

## 4. Results

Equations (8)–(10) have been solved numerically (by neglecting the implicit term $V_{pv} \cdot \nabla E$ in eq. (10) and neglecting the electron gyro-radius correction) for an initial equilibrium profile representing a plasma edge (see Fig. 1).

$$n_i = \tfrac{1}{2}(1 + \tanh(0.8y)). \tag{24}$$

The length of the slab is $L_x = 20$ in the periodic direction and extends from $y = -8$ to $y = 8$ in the transverse direction. A grid of 128 points in $y$ and 128 points in $x$ is used. Normalization is such that velocities are normalized to the ion thermal velocity $v_{thi}$, length is normalized to the gyro-radius $r_i = v_{thi}/\Omega_i$, and time is normalized to $\Omega_i^{-1}$. The potential is normalized to $T/e$, where $T$ is the temperature (we assume electrons and ions to have the same constant temperature). We use a time-step $\Delta t = 0.05$.

The initial ion density $\bar{n}_i$, which includes the finite gyro-radius correction as defined in eq. (4), is calculated from eq. (24) for the ions and is shown in Fig. 1 in dotted lines. Since the system is periodic in the $x$ direction and finite in the $y$ direction, we convolute the function in eq. (4) by first mirroring the function at the right boundary and thus doubling the interval. We then take the Fourier transform and multiply the coefficients by $\exp(-k^2 r_i^2/2)$, and then the function is Fourier transformed back. (Finite gyro-radius effects of the electrons are neglected). We take initially the electron density $n_e = \bar{n}_i$ at the plasma edge, so that the plasma is initially neutral. We run the code with $\nu_e = \nu_i = 7 \times 10^{-5}$. The time evolution of the system is conserving its initial neutrality, and the initial equilibrium is conserved. No charge separation is created at the plasma edge. (The invariant in eq. (7) is conserved). However, as soon as $\nu_e$ is set different from $\nu_i$, a charge separation is created at the edge of the plasma. We show in Figs (2)–(4) at different time the charge, the velocity $V_x(y) \sim E_y$ and the potential spatially averaged over the periodic direction $x$, for $\nu_e = 1 \times 10^{-4}$ and $\nu_i = 7 \times 10^{-5}$ (full curves) and $\nu_e = 7 \times 10^{-5}$, $\nu_i = 1 \times 10^{-4}$ (dotted curved). The charge spatially averaged over the periodic direction $x$, is constantly increasing (Fig. 2), together with the associated potential (Fig. 4) and the associated electric field $E_y$ (Fig. 3, $V_x(y) \sim E_y(y)$). However the time evolution of the Fourier modes in Fig. 5 remaining at the level of round-off errors shows a stable evolution in time. It is interesting to note the accuracy and stability of the numerical results. The case with $\nu_e = 2 \times 10^{-4}$ and $\nu_i = 7 \times 10^{-5}$ shows another evolution. Figs (6)–(8) gives the profiles, spatially averaged over the periodic direction $x$, of the charge, velocity $V_x(y) \sim E_y$ and the potential, and Fig. 9 gives the time evolution of the first three Fourier modes. The fundamental mode in Fig. 9 shows a rapidly growing instability at $t \sim 1000$, while the mode $k = 2k_0$ show an instability growing rapidly at $t \sim 4000$, (Fig. 9) and the

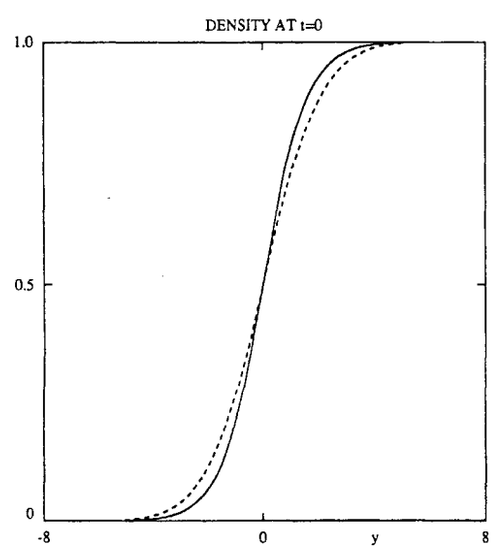


*Fig. 1.* Gyro-averaged ion density profile $\bar{n}_i$ calculated from eqs (4) and (24), as function of the transverse dimension $y$ (dotted curve), together with the profile in eq. (24) (full curve).

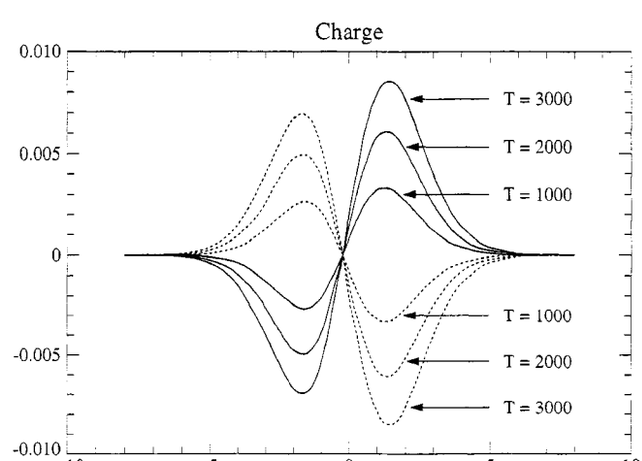


*Fig. 2.* Profile of the charge, spatially averaged over the periodic direction $x$, at (a) $t = 1000$; (b) $t = 2000$; (c) $t = 3000$; for the case $\nu_e = 1 \times 10^{-4}$, $\nu_i = 7 \times 10^{-5}$ (full curve) and $\nu_e = 7 \times 10^{-5}$, $\nu_i = 1 \times 10^{-4}$ (dotted curve).

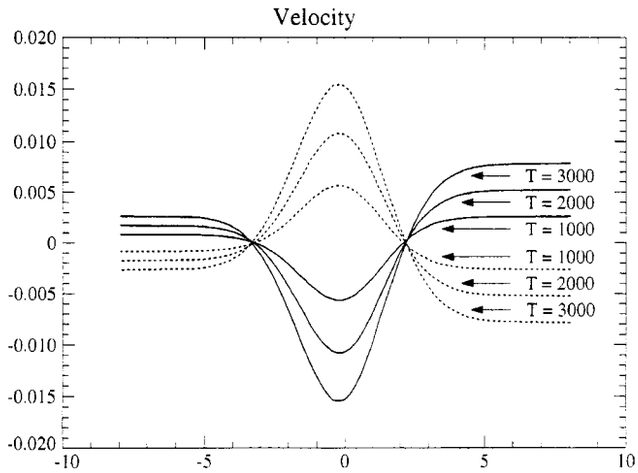


*Fig. 3.* Profile of the velocity $V_x(y) \sim E_y(y)$, spatially averaged over the periodic direction $x$, at (a) $t = 1000$; (b) $t = 2000$; (c) $t = 3000$; for the case, $v_e = 1 \times 10^{-4}$, $v_i = 7 \times 10^{-5}$ (full curve) and $v_e = 7 \times 10^{-5}$ and $v_i = 1 \times 10^{-4}$ (dotted curve).

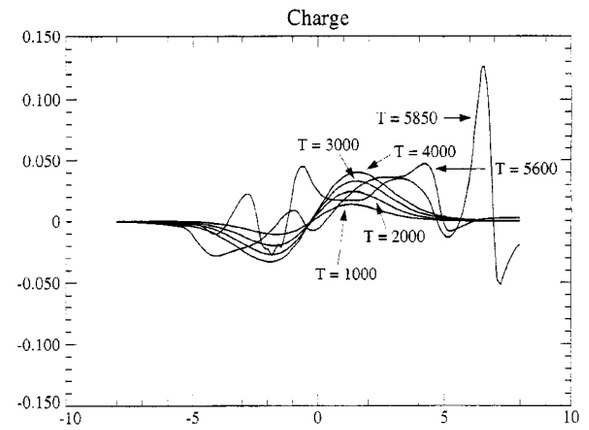


*Fig. 6.* Profile of the charge spatially averaged over the periodic direction $x$, at (a) $t0 = 1000$; (b) $t = 2000$; (c) $t = 3000$; (d) $t = 4000$; (e) $t = 5600$;(f) $t = 5850$ for the case $v_e = 2 \times 10^{-4}$.

mode $k = 3k_0$ follows at $t \sim 4300$. (Fig. 9). Although in this case $v_e$ has increased by a factor of 2 with respect to the previous case, the charge separation at $t = 1000$, 2000 and 3000 in Fig. 6 are much higher than a simple factor of 2 with respect to the corresponding ones in Fig. 3. When the instability is reaching a level where it is affecting the equilibrium, the charge is redistributing itself in Fig. 6 in such a way that the potential in Fig. 8 is distorting itself from a

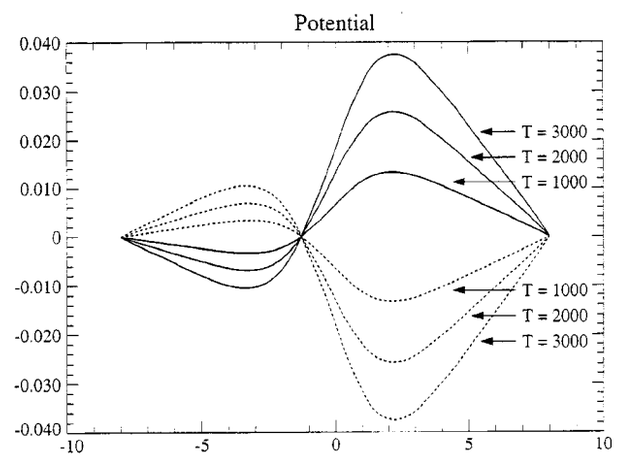


*Fig. 4.* Profile of the potential, spatially averaged over the periodic direction $x$, at (a) $t = 1000$; (b) $t = 2000$; (c) $t = 3000$; for the case $v_e = 1 \times 10^{-4}$, $v_i = 7 \times 10^{-5}$ (full curved) and $v_e = 7 \times 10^{-5}$, $v_i = 1 \times 10^{-4}$ (dotted curve).

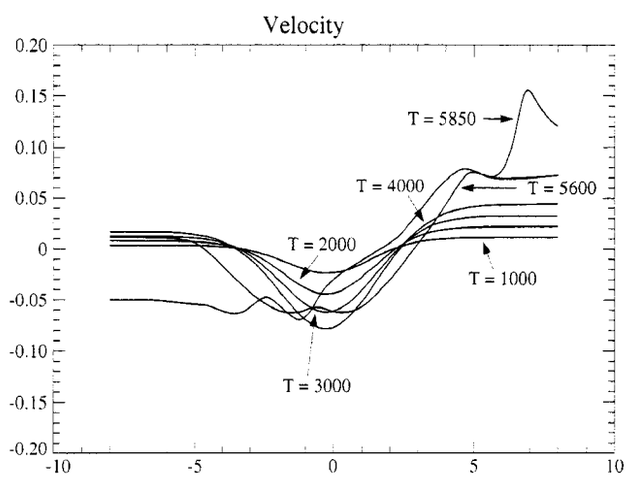


*Fig. 7.* Profile of the velocity $V_x(y) \sim E_y(y)$, spatially averaged over the periodic direction $x$, (a) $t = 1000$; (b) $t = 2000$; (c) $t = 3000$; (d) $t = 4000$; (e) $t = 5600$; (f) $t = 5850$ for the case $v_e = 2 \times 10^{-4}$.

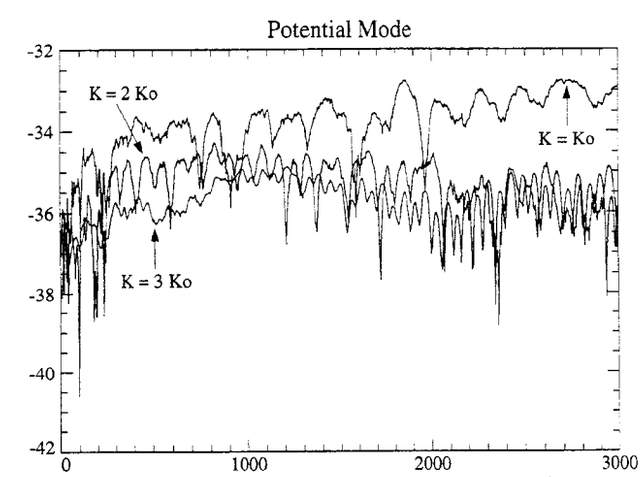


*Fig. 5.* Time evolution of the first three Fourier modes: (a) $k = k_0$; (b) $k = 2k_0$; (c) $k = 3k_0$ for the case $v_e = 1 \times 10^{-4}$, $v_i = 7 \times 10^{-5}$.

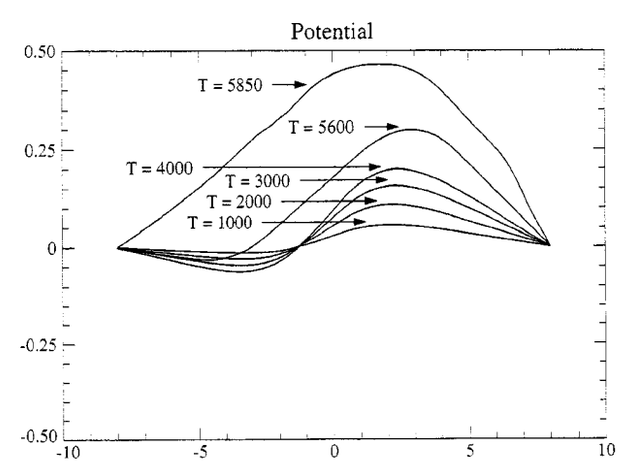


*Fig. 8.* Profile of the velocity $V_x(y) \sim E_y(y)$, spatially averaged over the periodic direction $x$, (a) $t = 1000$; (b) $t = 2000$; (c) $t = 3000$; (d) $t = 4000$; (e) $t = 5600$; (f) $t = 5850$ for the case.

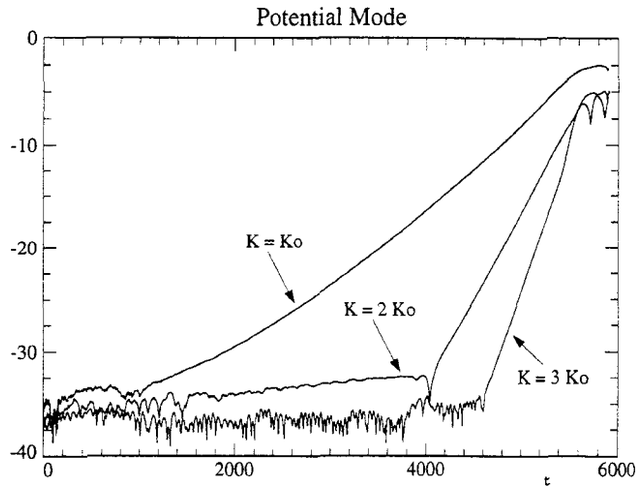


*Fig. 9.* Time evolution of the first three Fourier modes: (a) $k = k_0$; (b) $k = 2k_0$; (c) $k = 3k_0$ for the case $v_e = 2 \times 10^{-4}$.

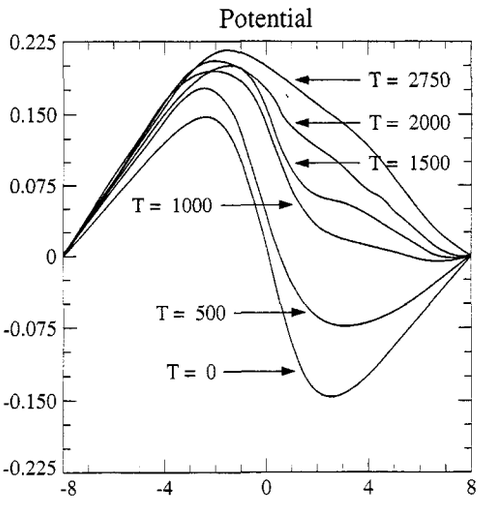


*Fig. 10.* Profile of the potential, spatially averaged over the periodic direction $x$, at (a) $t = 0$; (b) $t = 500$; (c) $t = 1000$; (d) $t = 1500$; (e) $t = 2000$; (f) $t = 2750$ ($v_e = 2 \times 10^{-4}$ and initially $n_e = n_i$).

sine like shape to the longest wavelentgh available in the system (a half-sine like structure), satisfying the boundary conditions, an evolution caracteristic of an inverse cascade (see the potential in Fig. 8 at $t = 5600$ and $t = 5850$).

Another set of runs was effected in which the potential had initially a sine-like shape similar to what we have seen in the previous set of parameters. This is constructed as follows. The initial ion density $\bar{n}_i$, which includes the finite gyro-radius correction as defined in eq. (4), is calculated from eq. (24) for the ions and is shown in Fig. 1 in dotted lines, and the initial electron density is taken to be $n_i$ as in eq. (14) (full curve in Fig. 1), instead of $\bar{n}_i$ as in the previous cases. The plasma is then initialy non-neutral. Due to this finite gyro-radius correction, there is an initial charge separation due to the difference $(\bar{n}_i - n_e)$ at the plasma edge, and the potential is calculated from Poisson equation eq. (21). Note that this charge separation (due only to the finite gyro-radius effect of the ions), is more important in the region where the guiding-center density gradient is important (the edge of a plasma for instance) rather than the region where the density is flat. This can be verified from eq. (4): a flat density profile does not lead to charge separation due to the finite Larmor radius effect. The initial velocity profile for the initial equilibrium profiles shown in Fig. 1, written in our normalized units as:

$$V_x(y) = E_y(y)/\omega_{pi} \tag{25}$$

where $E_y$ is the $y$ component of the electric field, has a bell-shaped gaussian. The initial shear is uniform in the $x$ direction. (Note that $\omega_{pi}$ is normalized to $\Omega_i$; in the present calculation we take $\omega_{pi} = 1$). For this initial equilibrium, $V_p \sim d\boldsymbol{E}/dt = 0$. We ran the code for this initial equilibrium (without any initial perturbation) for several thousands time-steps, (with $\Delta t = 0.05$). The equilibrium was exactly conserved, together with the invariants given in eq. (7) and the energy. The finite gyro-radius effect alone is providing the necessary charge separation at the plasma edge, and the self-consistent electric field provides the shear in the velocity at the plasma edge, through eq. (25). We can easily verify that any charge separation which is function of one space variable ($y$) is an equilibrium solution to the set of eqs. (8) if $v_e = v_i = 0$. Figure 10 shows the initial potential (averaged over the periodic dimension $x$), as a function of the transverse dimension $y$. This potential has, at $t = 0$ a sine-like shape, close to the shapes created in the previous set of runs. In the present simulation we impose a boundary value of zero on the potential at $y = -8$ and $y = +8$, in the solution of Poisson's equation (eq. (21)).

Adding an initial small perturbation $\sim(1 + \varepsilon \cos k_0 x)$ to the electron density changes this picture. We take $\varepsilon = 0.0025$ and $k_0 = 2\pi/L_x$. Figure 10 shows the shape of the spatially averaged potential evolving in such a way that the profile is taking a shape which has only a single maximum in the center, and satisfy the boundary conditions. This transition is well underway at $t = 1000$, and is completed at $t = 2000$ (Fig. 4). The evolution is in such a way that the Fourier modes spectrum of the potential is dominated by the fundamental mode (even when higher harmonics are excited in the initial perturbation), corresponding to the longest wavelength allowed in the transverse $y$ direction and by the periodic boundary condition in the $x$ direction. Figure 11 shows the time evolution, on a logarithmic scale, of the fundamental Fourier mode of the potential, showing growth followed by saturation (higher order harmonics remained

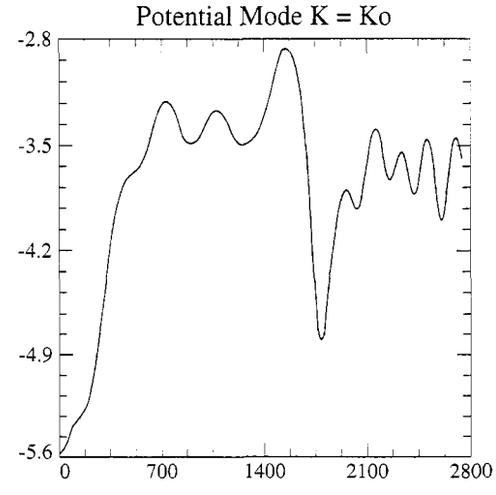


*Fig. 11.* Time evolution of the fundamental Fourier mode of the potential for $v_e = 2 \times 10^{-4}$, $v_i = 7 \times 10^{-5}$, for the case with an initial charge separation at $t = 0$. ($n_e = n_i$)

two order of magnitudes lower). This calculation is effected for $v_e = 2 \times 10^{-4}$ and $v_i = 7 \times 10^{-5}$. Note from Fig. 10 the peak of the potential varies very little from $t = 1000$ to $t = 2750$. From the results in Fig. 9, we can assert that the charge separation accentuated due to the difference between $v_e = 2 \times 10^{-4}$ and $v_i = 7 \times 10^{-5}$ as previously discussed, is still small at $t = 3000$, and the evolution shown in Fig. 11 reflects essentially the physics of an inverse cascade associated with the system, with the viscosity term smoothing the microstructures to avoid numerical instability.

We further increase the value of $v_e$ to $3 \times 10^{-4}$, all other parameters remaining constant. Figure 12 gives the time evolution on a logarithmic scale of the fundamental Fourier mode. After t = 2000, there is a rapid burst in the growth of the fundamental Fourier mode. The charge separation created by the difference in the electron and ion viscosities is unstable, and this instability is reaching a level where it is completly modifying the evolution of the system. The evolution of the potential profile, spatially averaged over the periodic distance $x$, is shown in Fig. 13. Up to $t = 2000$, the results are close to those previously reported Fig. 10: the potential is inverting itself to a half-sine like profile. The peak in Fig. 13 is close to the corresponding peak in Fig. 10,

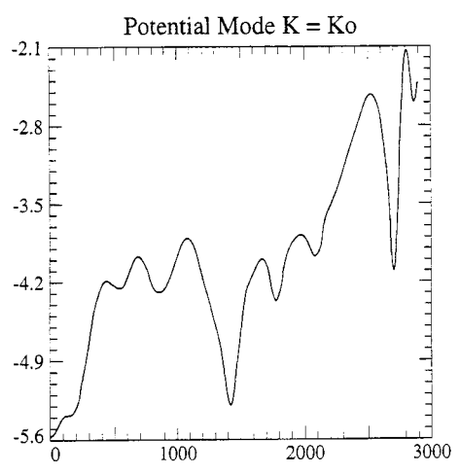


*Fig. 12.* Time evolution of the fundamental Fourier mode of the potential for $v_e = 3 \times 10^{-4}$, $v_i = 7 \times 10^{-5}$, for the case with an initial charge separation at $t = 0$. ($n_e = n_i$)

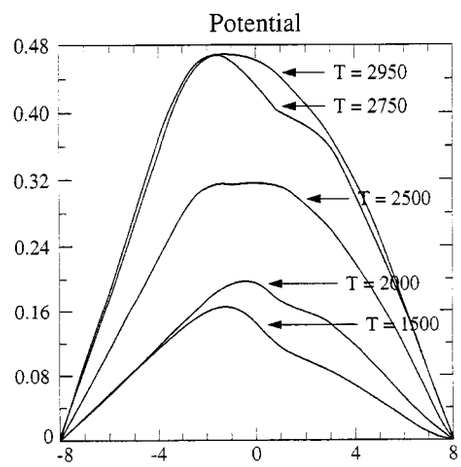


*Fig. 13.* Profile of the potential, spatially averaged over the periodic direction $x$, at (a) $t = 1500$; (b) $t = 2000$; (c) $t = 2500$; (d) $t = 2750$; (e) $t = 2950$.

in agreement with the fact that, $v_e$ has been slightly increased. This phase however, is followed by a rapid growth of the potential (see the peak at $t = 2000$, and $t = 2750$ in Fig. 13). Then the peak seems to saturate (see Fig. 12 and Fig. 13). Figures 14 show the contour plots for the potential. After $t = 1500$, the shear which appears in the velocity profile (tangent to the potential or stream function contours) is more apparent, and dominates at the top and the bottom of the figure (which corresponds to the bottom and top of the density profile), as we can see from Fig. 14(b) at $t = 2950$. We show the contour plot for the electron

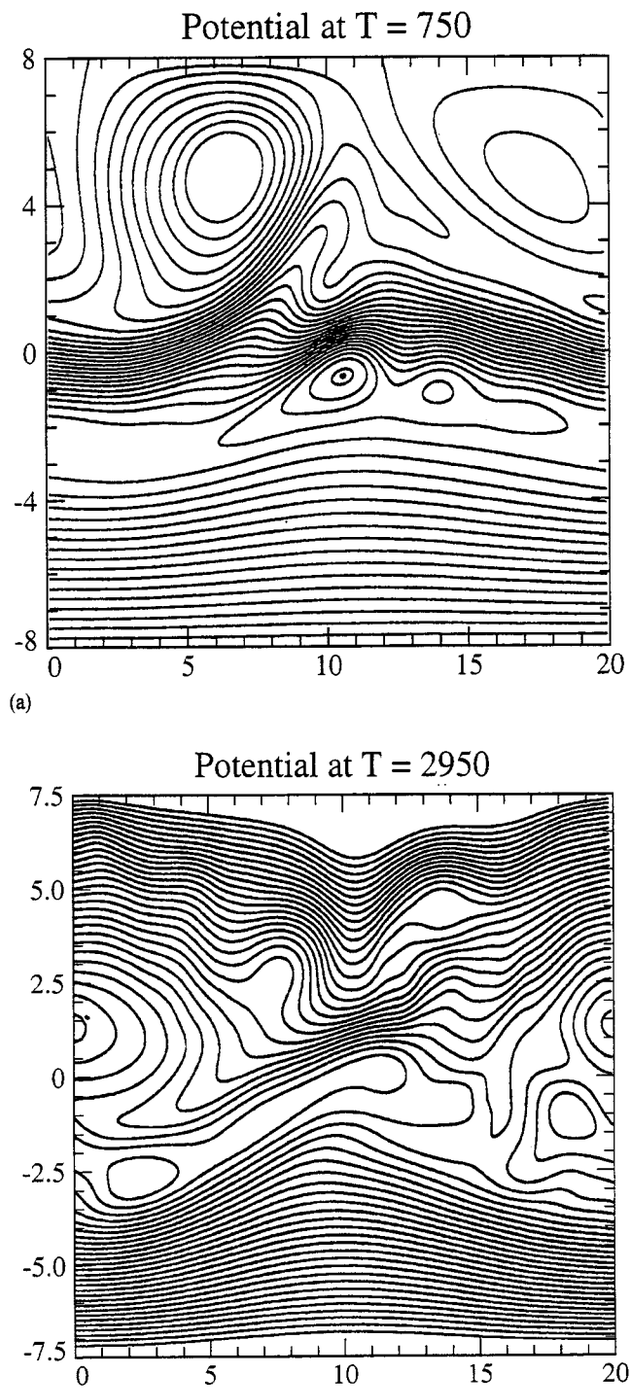


*Fig. 14.* Contour plots of the potential at (a) $t = 750$; (b) $t = 2950$. The potential is zero at $y = 8$ and the streamlines are essentially tangent to the line $y = 8$ with the exception of singular lines in Fig. (a) between two vortices, which are zero potential lines (hence connecting to the zero line at $y = 8$), in a transition between negative and positive potential contours.

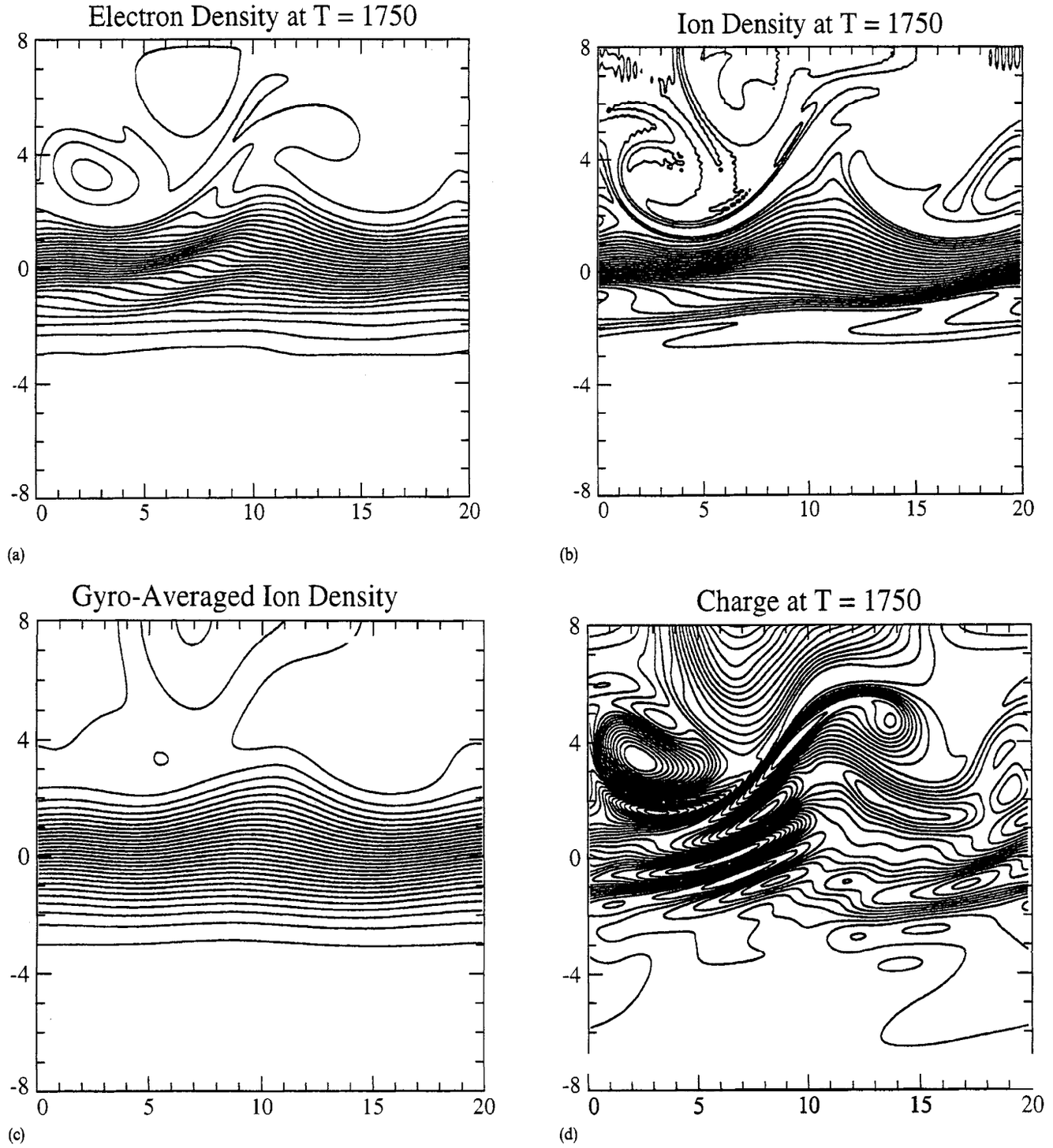


*Fig. 15.* Contour plots at $t = 1750$ for the case with $v_e = 3 \times 10^4$, for (a) electron density $n_e$; (b) ion density $n_i$; (c) gyro-averaged ion density $\bar{n}$; (d) charge $\rho = \bar{n}_i - n_e$. (The periodic direction $x$ is along the horizontal axis).

density $n_e$, the ion density $n_e$, the gyro-averaged ion density $\bar{n}_i$, and the charge $\rho = \bar{n}_i - n_e$ in Fig. 15 (at $t = 1750$, just before the rapid growth). In Fig. 16 (at $t = 2500$, during the rapid growth) we show the contour plot of the electron density and ion density. The smooth contours in the lower half of the density plots in Figs 15(a, b), are strongly twisted in Figs 16(a, b). We present the profiles at $t = 2950$, spatially averaged over the periodic direction $x$, of the electron density, the ion density, the gyro-averaged ion density in Fig. 17, and the velocity of the flow $V_x(y)$ in Fig. 18.

Two distinct phases of the evolution of the system appears in the cases we studied with an initial charge separation in the system:

(1) The first phase is the one where the initial profile unstable to an initial perturbation, is inverted or modified from a sine shape to a half-sine like shape and shear appears in the $V_x$ velocity profile.

(2) The second phase is the phase showing the rapid growth of the potential (and accordingly the $\boldsymbol{E} \times \boldsymbol{B}$ velocity, essentially tangent to the potential contours), with shear present in the velocity profile.

The shear in the flow is apparent from the contour plots of the potential (stream function). The velocity is tangent to the stream lines. The upper vortex structure in Fig 14(a) disappears and is replaced by a sheared flow in Fig. 14(b). The middle structure in Fig. 14(b) is the region where the direc-

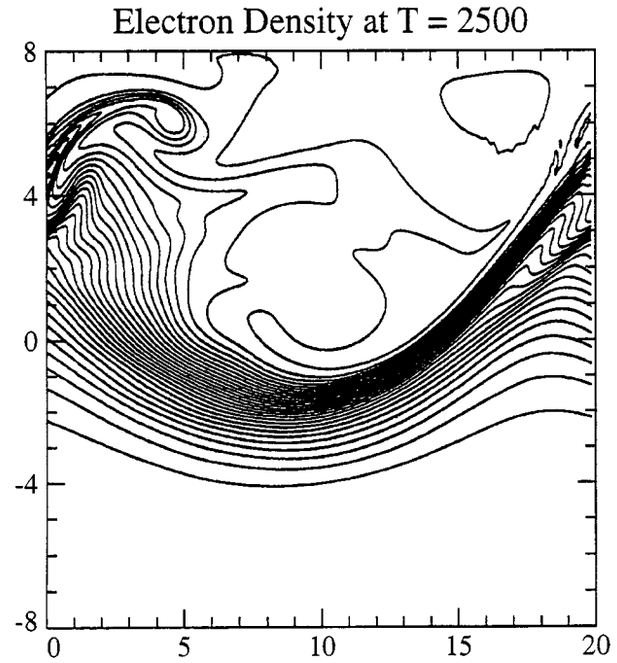


(a)

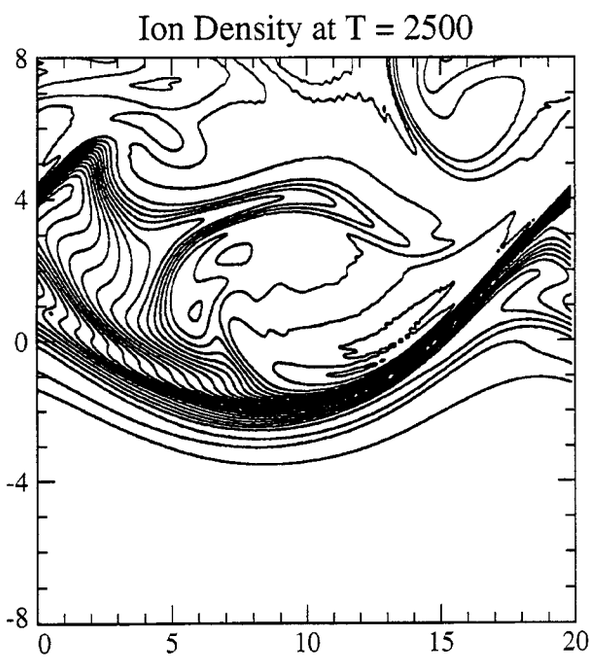


(b)

*Fig. 16.* Contour plots at $t = 2500$ for the case with $\nu_e = 3 \times 10^{-4}$, for (a) electron density $n_e$; (b) ion density $n_i$. (The periodic direction $x$ is along the horizontal axis).

tion of the flow (and the electric field since $V_x(y) \sim E_y(y)$) is changing sign.

## 5. Conclusions

A numerical code has been developed to study the generation of sheared flow at a plasma edge in the finite gyroradius guiding center approximation, which also included the polarization drift. The code apply a method of fractional steps, presented in Section 3, which has been previously applied with success to the Eulerian Vlasov codes. We have presented results which illustrates the accurate performance

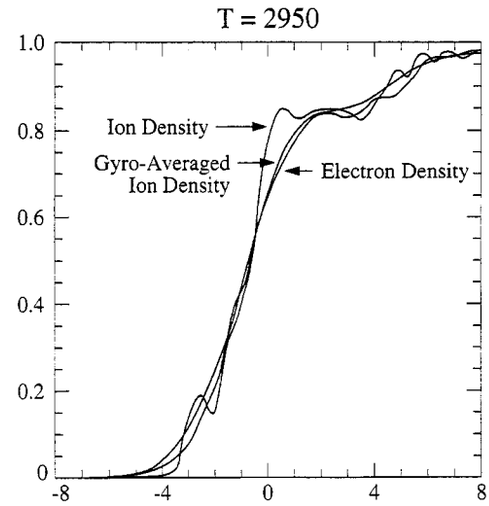


*Fig. 17.* Profiles, spatially averaged over the periodic direction $x$, for the case $\nu_e = 3 \times 10^4$ at $t = 2950$ for (a) electron density; (b) ion density; )c) gyro-averaged ion density.

of the code. In the physical model we are studying, the finite Larmor radius corrections allow for a charge separation to exist, and the polarization drift, which has different signs for ions and electrons, has tendency to accentuate a charge separation in a time varying electric field. We have included a viscosity term to study the effect of a small dissipation term on the solution and show how a difference in the viscous diffusion term, even small, can create a charge separation at the plasma edge of an initially neutral plasma. This charge separation can be unstable, and the instability saturates with energy evolving to the longest wavelength associated with the system, an evolution characteristic of an inverse cascade. The initial evolution of the system is essentially inviscid. We have also presented results for the case where the plasma is initially non-neutral. For this case, the evolution of the system shows, in the first phase, a behavior in accordance with some basic physics associated with the set of equations describing the behavior of guiding center plasma in a strong magnetic field [presented in eq. (8–10)], namely the inverse cascade with energy condensing in the lowest modes, while the system is evolving from an initial

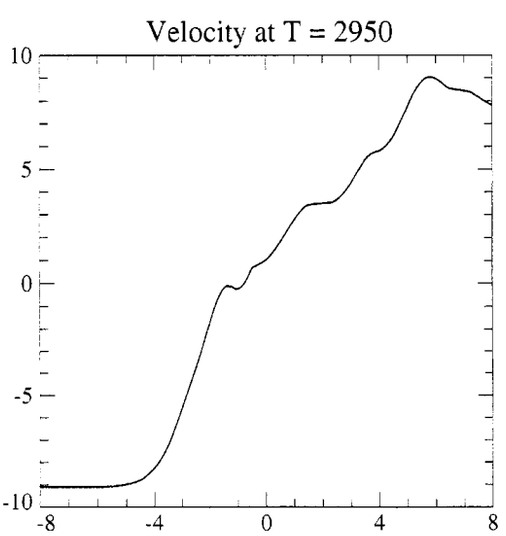


*Fig. 18.* Profile, spatially averaged over the periodic direction $x$, (for the case $\nu_e = 3 \times 10^{-4}$) for the velocity $V_x(y) \sim E_y(y)$, at $t = 2950$.

unstable flow with shear, through a stage showing complex structures with vortices, to a more stable shear dominated flow. The polarisation drift $\sim dE/dt$, plays an important role in this process, and also in triggering this instability. That the charge separation and the flow rearrange themselves via inverse cascades to adjust to a preferred state, as determined by boundary conditions and by the conservation properties associated with the model equations is one of the main points of the present results, and is based on a powerful statistical analysis of the model equations presented in Ref. [1]. In addition to these longest wavelength transition results, the sheared flow we are studying is generated at a plasma edge, and the formation and existence of a charge separation and an electric field at the plasma edge is studied self-consistently with the shear. (Two recent publications, Refs. [18–19], have attempted a theoretical study of the ions finite Larmor radius in this problem). The self-consistent results we are presenting are new, and certainly of relevance to edge plasma physics. Furthermore, it is generally admitted that velocity shear effects play an important role in suppressing turbulence. The present numerical results (supported by a strong theoretical analysis in Ref. [1]) suggest that inverse cascades (with energy condensing in the low $k$ modes) is a physical mechanism which can also play an important role in suppressing turbulence.

We have attempted to discriminate between the smoothing of the microstructure by a small viscous diffusion term to control numerical instabilities, and the modification of the macroscopic physical results introduced by this small viscous dissipation term. That the presence of a dissipation term is important to eliminate the small scale structure without affecting the large scales evolution of the system has been mentioned in several publications in connection with 2-D drift wave turbulence (Refs. [4–6]). However, it was pointed in connection with the 2-D guiding center equations in eq. (1) (see Ref. [3]), and in connection with 2-D magnetohydrodynamics (see Refs. [8–11]), that this viscosity term can play an important role in the evolution of the solution. (See also the comments in Ref. [20] on the results presented in Refs. [21–22]). We have presented results for a constant value of $\nu_i = 7 \times 10^{-5}$ showing how, when $\nu_e$ exceeds $2 \times 10^{-4}$ (for the set of parameters we have), the initial inviscid time evolution is followed by a stage in which the inverse cascade is accelerated, and then a very rapid growth of the potential and the associated velocity shear. The viscosity terms seem to play an important role in determining the asymptotic value of the electric field and the sheared velocity flow associated with the system. It is therefore our conclusions that very special attention has to be paid when a small viscous dissipation term is added with the objective of smoothing the microstructure and controling numerical instabilities.

The transition from a sheared flow to another shear dominated flow may be of importance to the problem of low to high or L-H transition and suppression of turbulence in the plasma edge in tokamaks. Steep density profiles in the vicinity of a separatrix accompanied by a strong radial electric field and poloidal rotation have been observed, with velocity profiles having large shear. Such a transition has also been observed in a Q-machine [23], indicating that L-H transitions (as essentially characterized by a higher velocity sheared flow and low turbulence) are not confined to toroidal plasmas. We make no claim in the present work to a study of the L-H transition with all its complexity. Although our computation is inspired by this experimental phenomenon, we believe that the results we are presenting for the existence of a charge separation and an electric field at a plasma edge due to the finite ions Larmor radius effect and viscous effects, with the charge adjusting in such a way that the largest available scales dominate, are pertinent and can stand on their own. Extending these results to models and parameters relevant to tokamak edge physics is underway.

## Acknowledgements

The CCFM is a joint venture of Hydro-Québec, the Government of Canada and the Institut National de la Recherche Scientifique, in which MPB Technologies Inc. and Canatom Inc. also participate.

## References

1. Knorr, G. and Pecseli, H. J. Plasma Phys. **41**, 157 (1989).
2. Knorr, G. and Shoucri, M. Proc. 19th European Physical Society Conf. on Plasma Physics, Innsbruck, 1992 (European Phys. Society), Vol. 16C, p. 00III-1721; J. Lebas, P. Bertrand, M. Shoucri, G. Knorr and A. Ghizzo, Proc. 20th European Physical Society Conf. on Plasma Physics, Lisbon, 1993 (European Phys. Society), Vol. 17C, p. II-815 (1993); M. Shoucri, *et al.* Proc. 22nd European Physical Society Conf. on Plasma Physics, Bournemouth, 1995 (European Phys. Society), Vol. 19c, p. IV-197 (1995).
3. Bertrand, P. C. R. Acad. Sc. Paris, 282, série B-275 (March 1976).
4. Smith, S. A. and Hammett, G. W. Proceedings of the 15th Numerical Simulation Conference, Valley Forge, Pennsylvania, 1994 (paper 3A6).
5. Camargo, S. J., Biskamp, D. and Scott, B. Proceedings of the 21st European Physical Society Conference on Plasma Physics, Montpellier, 1994 (European Phys. Society), Vol. 18B, p. 564.
6. Kinney, R. Williams, J.-C. and Tajima, T. Phys. Plasmas **2**, 3623 (1995).
7. Manfredi, G., Shoucri, M., Dendy, R., Ghizzo, A. and Bertrand, P. Phys. Plasmas **3**, 202 (1996).
8. Politano, H., Pouquet, A. and Sulem, P. Phys. Fluids **B1**, 2330 (1989).
9. Matthaeus, W. H. Proceedings in Solar Terrestial Physics: Presence and Future, Workshop edited by D. Butler and K. Papadopoulos, NASA Reference publication 1120 (NASA, Washington, DC, 1984) Chap. 1, p. 40.
10. Priest, E. P. Rep. Prog. Phys. **48**, 955 (1985).
11. Shan, X. and Montgomery, D. Phys. Rev. Lett. **73**, 1624 (1994); Plasma Phys. Control. Fusion **35**, 619 (1993); ibid **35**, 1019 (1993).
12. Seyler, C. E., Salu, T., Montgomery, D. and Knorr, G. Phys. Fluids **18**, 803 (1975).
13. Dorland, W. and Hammett, G. Phys. Fluids **B5**, 812 (1993).
14. Lee, W. Phys. Fluids **26**, 556 (1983).
15. Cheng, C. Z. and Knorr, G. J. Comp. Phys. **22**, 330 (1976); M. Shoucri and R. Gagné, J. Comp. Phys. **27**, 315 (1978).
16. Knorr, G., Joyce, G. and Marcus, A. J. Comp. Phys. **38**, 227 (1980).
17. Ghizzo, A., Bertrand, P., Schoucri, M., Fijalkow, E. and Feix, M. J. Comp. Phys. **108**, 105 (1993).
18. Hazeltine, R. D., Ziao, H. and Valanju, P. M. Phys. Fluids **B5**, 4011 (1993).
19. Tendler, M., Daybelge, V. and Rozhansky, V. in Proceedings of the 14th International Conference on Plasma Physics and Controlled Nuclear Fusion (Würzburg, 1992; Ed. International Atomic Energy Agency, Vienna) Vol. 2, p. 243.
20. Montgomery, D. and Matthaeus, W. H. Phys. Fluids **B5**, 657 (1993) and references therein.
21. Drake, J. F. *et al.* Phys. Fluids **B4**, 488 (1992).
22. Finn, J. M., Drake, J. F. and Guzdar, P. N. **B4**, 2758 (1992).
23. Huld, T., Nielsen, A. H., Pecseli, H. L. and Rasmussen, Y. Y. Phys. Fluids **B4**, 1609 (1991).

## Appendix I

*The Energy Theorem*

We assume the plasma is governed by the eqs (6), (7) and (8). Even though the finite Larmor radius for electrons is usually neglected, we show that the time derivative of $\frac{1}{2}\int V_D^2\,dt$ for finite ion and electron Larmor radii can be represented as time derivatives and divergence terms, the latter vanishing if appropriate boundary conditions are chosen.

$$I = \frac{\partial}{\partial t}\frac{1}{2}\int V_D^2\,d\tau = \frac{\partial}{\partial t}\frac{1}{2}\int \nabla\dot{\phi}\cdot\nabla\phi\,d\tau$$

$$= \frac{1}{B^2}\int \nabla\cdot(\phi\nabla\dot{\phi})\,d\tau - \frac{1}{B^2}\int \phi\nabla^2\dot{\phi}\,d\tau. \tag{A.1}$$

(the dot denotes time derivative).

The time derivative of the Poisson equation and the continuity equations give

$$I = \frac{q}{\varepsilon_0 B^2}\int \phi(\bar{n}_i^i - \bar{n}_e^e)\,d\tau = -\frac{q}{\varepsilon_0 B^2}$$

$$\times \int \phi\nabla\cdot g_i \otimes [(\bar{V}_{Di}^i + \bar{V}_{pi}^i)n_i]\,d\tau$$

$$+ \frac{q}{\varepsilon_0 B^2}\int \phi\cdot g_e \otimes [(\bar{V}_{De}^i + \bar{V}_{pe}^e)n_e]\,d\tau. \tag{A.2}$$

Note that the convolution process indicated by the tilde or the operator $g\otimes$ takes place twice, due to the modified velocities and densities. Convolution and differential operators commute and the second convolution can be shifted to the other member of the product.

Consider the first integral on the right hand side

$$\int \phi g_i \otimes \nabla\cdot(\bar{V}_{Di}^i + \bar{V}_{pi}^i)n_i\,d\tau = \int \bar{\phi}^i\nabla\cdot(\bar{V}_{Di}^i + \bar{V}_{pi}^i)n_i\,d\tau$$

$$= \int \nabla\cdot(\bar{\phi}^i\bar{V}_{Di}^i n_i)\,d\tau - \int \nabla\bar{\phi}^i\cdot\bar{V}_{Di}^i n_i\,d\tau$$

$$- \int \bar{\phi}^i\nabla\cdot(\bar{V}_{pi}^i n_i)\,d\tau \tag{A.3}$$

The first and second integrals vanish and the third becomes

$$-\int \nabla\cdot(\bar{\phi}^i\bar{V}_{pi}^i n_i)\,d\tau + \int \nabla\bar{\phi}^i\cdot\bar{V}_{pi}^i n_i\,d\tau. \tag{A.4}$$

Using the definition of the polarization drift, we obtain

$$-\alpha_i\int \nabla\bar{\phi}^i\cdot\left[\frac{\partial}{\partial t}\bar{E}^i + (\bar{V}_{Di}^i + \bar{V}_{pi}^i)\cdot\bar{E}^i\right]n_i\,d\tau$$

$$= \alpha_i\int n_i\frac{\partial}{\partial t}(\tfrac{1}{2}\bar{E}^{i2})\,d\tau + \alpha_i\int(\bar{V}_{Di} + \bar{V}_{pi})\cdot\nabla(\tfrac{1}{2}\bar{E}^{i2})n_i\,d\tau$$

$$= \alpha_i\int\left\{\frac{\partial}{\partial t}(\tfrac{1}{2}n_i\bar{E}^{i2})\,d\tau - \frac{\bar{E}^{i2}}{2}\frac{\partial}{\partial t}n_i\right.$$

$$+ \nabla\cdot[n_i(\bar{V}_{Di} + \bar{V}_{pi})\tfrac{1}{2}\bar{E}^{i2}]$$

$$\left. - \tfrac{1}{2}\bar{E}^{i2}\nabla\cdot[n_i(\bar{V}_{Di} + \bar{V}_{pi})]\right\}d\tau. \tag{A.5}$$

With the surface terms vanishing again, this becomes

$$\alpha_i\int\left\{\frac{\partial}{\partial t}(n_i\,\tfrac{1}{2}\bar{E}^{i2}) - \frac{(\bar{E}^i)^2}{2}\frac{\partial}{\partial t}n_i + \frac{(\bar{E}^i)^2}{2}\left(\frac{\partial}{\partial t}n_i\right)\right\}d\tau$$

$$= \alpha_i\frac{\partial}{\partial t}\int(\tfrac{1}{2}n_i(\bar{E}^i)^2)\,d\tau. \tag{A.6}$$

The electron integral is of the same structure so that we obtain

$$\frac{\partial}{\partial t}\int\frac{1}{2}\left[V_D^2 + \frac{q_i^2}{\varepsilon_0 m_i B^2\Omega_i^2}n_i(\bar{E}^i)^2 + \frac{q_e^2}{\varepsilon_0 m_e B^2\Omega_e^2}n_e(\bar{E}^e)^2\right]d\tau = 0. \tag{A.7}$$

Multiplying by $\varepsilon_0 B^2$ and integrating in time, we obtain the energy theorem in the form

$$\frac{1}{2}\int\left[\varepsilon_0 E^2 + \left(\frac{\omega_{pi}}{\Omega_i}\right)^2\frac{n_i}{n_0}(\bar{E}^i)^2 + \left(\frac{\omega_{pe}}{\Omega_e}\right)^2\frac{n_e}{n_0}(\bar{E}^e)^2\right]d\tau$$

$$= \text{const.} \tag{A.8}$$